Improving $PM_{2.5}$ Forecasts in China Using an Initial Error Transport Model

Huangjian Wu,[,†] Xiaogu Zheng,[‡] Jiang Zhu,[‡,§] Wei Lin,[*,‖] Haitao Zheng,[⊥] Xueshun Chen,[#,Δ] Wei Wang,[○] Zifa Wang,[#,§,Δ] and Song Xi Chen[†]*

[†]Guanghua School of Management and Center for Statistical Science, Peking University, Beijing 100871, China

[‡]CAS-TWAS Center of Excellence for Climate and Environment Sciences, Institute of Atmospheric Physics, Chinese Academy of Sciences, Beijing 100029, China

[§]University of Chinese Academy of Sciences, Beijing 100049, China

[‖]School of Mathematical Sciences and Center for Statistical Science, Peking University, Beijing 100871, China

[⊥]Key Laboratory of Environmental Optics and Technology, Anhui Institute of Optics and Fine Mechanics, Chinese Academy of Sciences, Hefei, Anhui 230031, China

[#]State Key Laboratory of Atmospheric Boundary Layer Physics and Atmospheric Chemistry, Institute of Atmospheric Physics, Chinese Academy of Sciences, Beijing 100029, China

[Δ]Center for Excellence in Regional Atmospheric Environment, Institute of Urban Environment, Chinese Academy of Sciences, Xiamen, Fujian 361021, China

[○]China National Environmental Monitoring Center, Beijing 100012, China

ABSTRACT

The efforts of using data assimilation to improve $PM_{2.5}$ forecasts have been hindered by the limited number of species and incomplete vertical coverage in the observations. The common practice of initializing a chemical transport model (CTM) with assimilated initial conditions (ICs) may lead to model imbalances, which could confine the impacts of assimilated ICs within a day. To address this challenge, we introduce an Initial Error Transport Model (IETM) approach to improving $PM_{2.5}$ forecasts. The model describes the transport of initial errors by advection, diffusion, and decay processes, and calculates the impacts of assimilated ICs separately from the CTM. The CTM forecasts with unassimilated ICs are then corrected by the IETM output. We implement our method to improve $PM_{2.5}$ forecasts over central and eastern China. The reduced root-mean-square errors for 1- to 4-day forecasts during January 2018 are 51.2, 27.0, 16.4, and 9.4 μg m^{-3}, respectively, which are 3.2, 6.9, 8.6, and 10.4 times those by the CTM forecasts with assimilated ICs. More pronounced improvements are found for highly reactive $PM_{2.5}$ components. These and similar results for July 2017 suggest that our method can enhance and extend the impacts of the assimilated data without being affected by the imbalance issue.

INTRODUCTION

Air quality forecasting is essential for developing short-term air pollution control strategies and mitigating health risks from air pollution.[1] Substantial forecast errors, however, may be induced by uncertainties in the initial concentrations, emissions, and physical and chemical processes, possibly leading to false alarms or missed episodes of pollution events.[2] Owing to the fast economic growth and implementation of increasingly stringent emission control policies in China, the rapid changes in emissions are usually not captured by the slowly updated emission inventories, posing further challenges to air quality forecasting in China.[3]

Various data assimilation techniques, including optimal interpolation (OI),[4] four-dimensional variational assimilation (4D-Var),[5] and ensemble Kalman filter (EnKF),[6] have been adopted to improve air quality forecasts. It is standard practice to supply initial conditions (ICs) directly to a chemical transport model (CTM) with the assimilated data.[7] This assimilated model initialization approach has proved effective in improving air quality forecasts by assimilating diverse types of observations such as in situ, remote sensing, and satellite data.[8-10] Despite these considerable successes, the benefits of data assimilation may not be fully exploited. Ma et al.[11] assimilated surface in situ $PM_{2.5}$ observations to improve 3-day $PM_{2.5}$ forecasts and found that most improvements by the assimilated ICs were limited to within the first day of the forecast; similar conclusions were drawn from other studies when only surface $PM_{2.5}$ observations are assimilated.[12,13] By contrast, it is estimated that the global average residence time of accumulation-mode aerosols (0.1-2 μm diameter) emitted near the surface falls in the range of three to seven days.[14,15] This discrepancy between the residence time of aerosols and the duration of the impacts of assimilated ICs suggests that $PM_{2.5}$ forecasts can be further improved.

There are two types of imbalances that have hindered the improvement by using assimilated ICs for model initialization. First, the number of assimilated species is often limited, resulting in the imbalance between the assimilated and unassimilated variables.[16] Also, the incomplete vertical coverage of the assimilated data (e.g., by assimilating only surface observations) may lead to the imbalance in space.[17] By model initialization, these imbalances will be brought into the CTM and generate spurious species interactions and vertical transport, which in turn degrade the forecasting performance.[18] Although this model imbalance issue is rarely discussed in the air quality forecasting literature, some previous studies have indicated that $PM_{2.5}$ forecasts can be improved by extracting more observational information across space and chemical species. For example, Schwartz[19] showed that better forecasts were achieved by simultaneously assimilating surface $PM_{2.5}$ observations and satellite aerosol optical depth (AOD) retrievals. Moreover, it has been found that 2- to 3-day forecasts of $PM_{2.5}$ can be significantly improved by assimilating multi-species surface chemical observations (e.g., $PM_{2.5}$, SO_2, and NO_2).[8,20]

Model imbalances due to initialization, or initialization shocks, have been well recognized and explored in numerical weather prediction and ocean modeling.[21,22] Several procedures to mitigate the initialization shock and increase the dynamical balance have been developed. These include, among others, pre- and post-processing methods such as nonlinear normal mode initialization[23,24] and digital filtering,[25] as well as incremental analysis update schemes that gradually introduce the analysis increments over a time window.[26] Although these initialization techniques are effective in reducing spurious high-frequency oscillations, they do not completely eliminate the imbalances and can partially undo the efforts of data assimilation.[27,28]

In this study, we suggest a new way to extract information from the assimilated ICs without bringing the imbalances into the CTM, and introduce an Initial Error Transport Model (IETM) approach to improving $PM_{2.5}$ forecasts. The model describes the transport of errors from the ICs by advection, diffusion, and decay processes, and calculates the impacts of assimilated ICs separately from the CTM. The CTM forecasts with unassimilated ICs are then corrected by the IETM output. We implement and test our method on $PM_{2.5}$ forecasts over central and eastern China during January 2018 and July 2017. The reductions in root-mean-square error (RMSE) for 4-day forecasts were still apparent, substantially improving results from direct initialization of the CTM. Reasons that explain the improvements are also discussed.

METHODS AND DATA

IETM Methodology

Our model for describing the transport of initial errors is motived by the fundamental principles and major components of the governing equations for CTMs. A generic form of the governing equation for a pollutant of interest is given by

$$\frac{\partial c^{\mathrm{f}}}{\partial t} = \nabla \cdot \left(K^{\mathrm{f}} \nabla c^{\mathrm{f}}\right) - \nabla \cdot \left(\boldsymbol{v}^{\mathrm{f}} c^{\mathrm{f}}\right) + E^{\mathrm{f}} + R^{\mathrm{f}}\left(c^{\mathrm{f}}\right) + D^{\mathrm{f}}\left(c^{\mathrm{f}}\right) \qquad (1)$$

where c^{f} is the pollutant concentration, K^{f} is the eddy diffusivity, $\boldsymbol{v}^{\mathrm{f}}$ is the wind vector, and E^{f}, R^{f}, and D^{f} are the changes of concentrations resulting from the emission, reaction, and deposition processes, respectively. Here the superscript "f" stands for "forecast." Equation 1 explicitly models the diffusion and advection processes, while leaving the other components nominally defined. Air quality forecasts are then obtained by solving the equation numerically with appropriate ICs. Conventionally, assimilated ICs with less bias and higher accuracy are supplied directly to the CTM. This approach, however, also brings imbalances in the assimilated ICs into the CTM, resulting in model imbalances and limiting the benefits of assimilated ICs.

We next derive a governing equation for the forecast errors. Suppose that the true concentrations follow the same form of governing equation as eq 1:

$$\frac{\partial c^*}{\partial t} = \nabla \cdot \left(K^* \nabla c^*\right) - \nabla \cdot \left(\boldsymbol{v}^* c^*\right) + E^* + R^*\left(c^*\right) + D^*\left(c^*\right) \qquad (2)$$

Define the forecast error by $e = c^{\mathrm{f}} - c^*$. To obtain an equation in terms of e only, we assume for simplicity that the eddy diffusivity and the wind vector are without error, that is, $K^{\mathrm{f}} = K^*$ and $\boldsymbol{v}^{\mathrm{f}} = \boldsymbol{v}^*$. In the presence of errors in K^{f} and $\boldsymbol{v}^{\mathrm{f}}$, the resulting equation will still be a good approximation, provided that these errors are relatively small. This assumption is reasonable, since diffusion is negligibly slow compared to advection[29] and wind forecasts are sufficiently accurate for up to 4 days.[30] Now, subtracting eq 2 from eq 1 gives the equation for the forecast error e:

$$\frac{\partial e}{\partial t} = \nabla \cdot \left(K^{\mathrm{f}} \nabla e\right) - \nabla \cdot \left(\boldsymbol{v}^{\mathrm{f}} e\right) + \Psi(c^{\mathrm{f}}, c^*) \qquad (3)$$

where

$$\Psi(c^{\mathrm{f}}, c^*) = E^{\mathrm{f}} + R^{\mathrm{f}}(c^{\mathrm{f}}) + D^{\mathrm{f}}(c^{\mathrm{f}}) - E^* - R^*\left(c^*\right) - D^*\left(c^*\right)$$

The first and second terms on the right-hand side of eq 3 are the diffusion and advection operators, respectively, which reflect the transport of forecast errors. Here the transported error refers to the error transported from the previous time step, which involves errors arising from all sources including emission, reaction, and deposition. Meanwhile, the last term Ψ in eq 3 represents the error arising from all uncertainties at the current time step. This part of error is generally difficult to estimate because it depends on the unknown true emission, reaction, and deposition processes. Fortunately, for $PM_{2.5}$ as a pollutant with a typical lifetime of 4 days in the lower troposphere,[31] the error generated at a single time step is relatively small compared to the transported error, as we will show in SI Figure S1 and the Results and Discussion section. A related work by Skachko et al.[32] found that transport plays a major role in describing the evolution of model error for data assimilation.

Although an explicit expression of Ψ in eq 3 is not available, the physical and chemical removal processes of the pollutant are expected to follow an exponential decay.[33] We thus approximate Ψ by a decay term and arrive at the governing equation for our initial error transport model (IETM):

$$\frac{\partial e}{\partial t} = \nabla \cdot \left(K^{\mathrm{f}} \nabla e\right) - \nabla \cdot \left(\boldsymbol{v}^{\mathrm{f}} e\right) - \alpha e \tag{4}$$

where α is a decay rate parameter that controls the lifetime of the forecast errors. This simplified equation can then be solved numerically. Although eq 4 depends on e only, solving the equation requires knowing the initial error $e_0 = c_0^{\mathrm{f}} - c_0^*$. Since c_0^* is unknown, we estimate it by the assimilated initial concentration. Finally, consider a baseline forecast c^{f} that is obtained by solving eq 1 with unassimilated ICs. In view of the relation $e = c^{\mathrm{f}} - c^*$ mentioned above, we correct the baseline forecast by subtracting the solution e^{i} to eq 4 and obtain our final forecast

$$c^{\mathrm{i}} = c^{\mathrm{f}} - e^{\mathrm{i}}$$

where the superscript "i" stands for the IETM approach.

To recap, the proposed IETM approach describes the transport of initial errors through a simplified governing equation consisting of diffusion, advection, and decay terms. The solution to this equation is then used to correct the baseline forecast from the full CTM with unassimilated ICs. Overall, the IETM methodology avoids breaking the model balances in the CTM by calculating the impacts of assimilated ICs separately from the CTM, thereby improving the final forecasts.

Numerical Implementation

We adopted the Nested Air Quality Prediction Modeling System (NAQPMS)[34] developed by the Institute of Atmospheric Physics, Chinese Academy of Sciences, as the CTM in this study. NAQPMS runs in three dimensions with 20 vertical layers; more details about NAQPMS are provided in Supporting Information (SI) Section S1. We used the method of optimal interpolation (OI) for data assimilation, which is described in SI Section S2. Differences between the unassimilated and assimilated ICs are treated as the ICs for the IETM. Numerical schemes and parameter settings for implementing the advection, diffusion, and decay processes in eq 4 are described as follows.

The advection process is calculated through a mass conservative, peak-preserving, mixing ratio bounded advection algorithm developed by Walcek and Aleksic.[35] The algorithm employs dual-linear segment approximations and a special treatment near the local maxima and minima to preserve extremes and reduce numerical diffusion. It has been widely used in CTMs to advect chemical species with nonnegative concentrations;[34,36,37] however, it does not require positive-definite initial fields, and negative quantities can be advected. A two-dimensional implementation of the scheme is described in SI Section S3 and applied for the horizontal advection of forecast errors. Vertical advection is not considered here for three reasons. First, only surface in situ observations are assimilated in this study, so that the assimilated concentrations in the surface layer are more accurate than those in higher layers. Second, vertical wind speeds are significantly smaller than horizontal wind speeds. Finally, omitting the vertical advection would introduce a relatively small error, but can save almost 90% of the computational cost.

The implementation of the diffusion process is straightforward except for determining the value of eddy diffusivity K^{f}. Sometimes, K^{f} is set to zero or an empirical constant because diffusion is negligibly slow compared to advection.[29] Here, it is calculated by a scheme based on model resolution and wind speed derivatives.[38]

The decay rate parameter α in eq 4 determines the lifetime of forecast errors. It has been shown that the lifetimes of components in $PM_{2.5}$ range from less than a day to a few weeks.[14] Here, we regard the lifetime of the impacts of initial errors as the same as the lifetime of $PM_{2.5}$, which is about 4 days in the lower troposphere.[31] Accordingly, α is set to the reciprocal of the lifetime, that is, 1/96 h^{-1}. As a result, the impacts of initial errors will last at least 4 days if not transported outside the simulation domain.

During forecasting, we run the full CTM once to obtain the baseline forecast, and run the IETM once to yield the correction. Compared with the conventional method that runs the CTM once with assimilated ICs, our method requires extra computation to run the IETM. However, the IETM is a two-dimensional, simplified model, which is easy and cheap to implement. Moreover, since the background forecast has already been obtained in the OI assimilation scheme, it can be used directly as the baseline forecast, thereby saving even more computation.

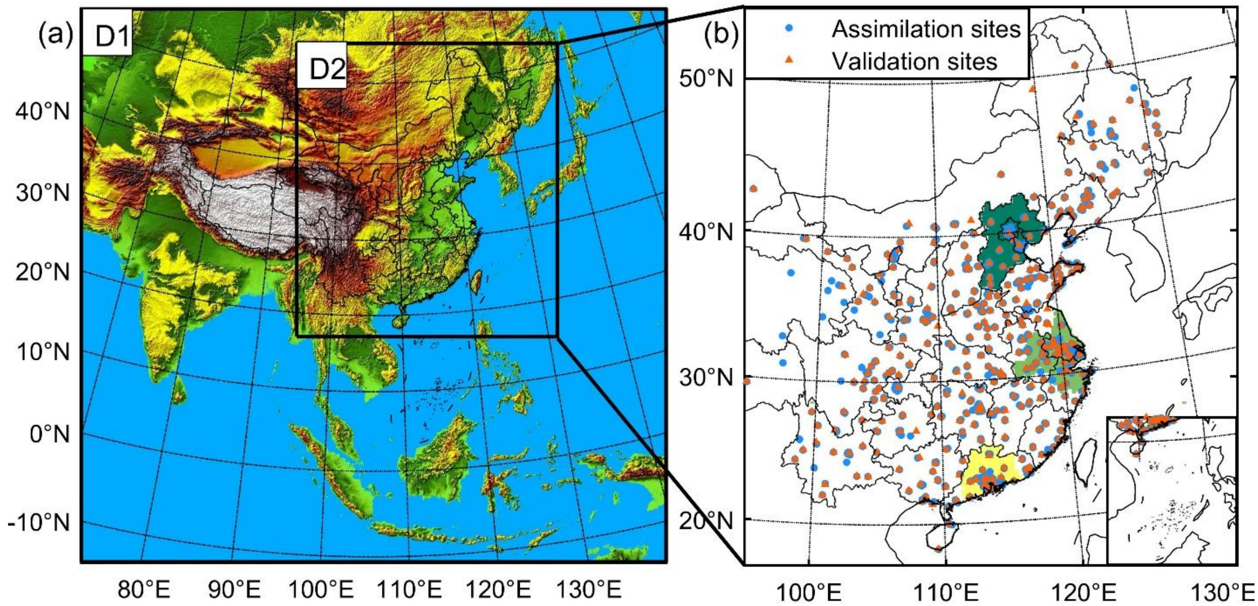

Figure 1. (a) Domain configurations and (b) distribution of monitoring sites. The outer domain (D1) covers East Asia at a 45 km horizontal resolution, and the inner domain (D2) covers central and eastern China at a 15 km horizontal resolution. Colored regions in (b) indicate the Beijing-Tianjin-Hebei, Yangtze River Delta, and Pearl River Delta regions from north to south.

Observational Data

The surface $PM_{2.5}$ observations used in this study were obtained from the China National Environmental Monitoring Center. These observations were first examined by a probabilistic automatic outlier detection method[39] to remove data with abnormally large representation or observational errors. After excluding sites with excessive missing or removed data, there were 1326 monitoring sites located in the research area as shown in Figure 1. Most of these sites were in urban areas and there was more than one monitoring site for most cities. To ensure that there was at least one assimilation site for each city, one validation site was randomly selected for cities with more than two available sites. A total of 1003 sites were selected for assimilation, among which 57 were located in the Beijing-Tianjin-Hebei (BTH) region, 120 in the Yangtze River Delta (YRD) region, and 59 in the Pearl River Delta (PRD) region. The other 323 sites were used for validation, including 13, 37, and 15 sites in the BTH, YRD, and PRD region, respectively.

Configurations of Forecasting Experiments

Three forecasting experiments were carried out to produce 96 h forecasts of $PM_{2.5}$ during January 2018 and July 2017. These experiments share the same domain configurations, emission inventories, meteorological initial and boundary conditions, and parameter settings for the CTM, with the only difference being the treatments of ICs as described below.

The first experiment supplies the unassimilated ICs, which are extracted from the forecasts started 24 h ago, directly to the CTM. The second experiment uses the assimilated ICs instead for the CTM. The third experiment implements the proposed method, which corrects the forecasts produced in the first experiment with the output from the IETM. The ICs for the IETM are obtained by subtracting the assimilated ICs from the unassimilated ICs. While the CTM includes 20 vertical layers, only surface $PM_{2.5}$ observations were obtained and assimilated in this study. The restart interval is set to 24 h and the assimilation frequency is hourly. Components of $PM_{2.5}$ in the assimilated ICs (e.g., nitrate, sulfate, organic aerosols, and black carbon) are adjusted proportionally to the change of total $PM_{2.5}$ before and after data assimilation.

RESULTS AND DISCUSSION

Transport of Forecast Errors

It is well documented that transport plays a major role in the evolution of $PM_{2.5}$.[40-42] The $PM_{2.5}$ driven by cold surges can travel up to 2000 km from northern to southern China within two days.[43] Moreover, components with longer lifetimes (e.g., dust and black carbon) can travel across oceans,[44] and intercontinental transport of aerosols is estimated to account for 36–97% of the background surface concentrations.[40]

Equation 3 suggests that the forecast errors of $PM_{2.5}$ can be similarly transported. Numerical evidence for such error transport from the forecasting experiments is shown in Figure 2 and SI Video S1. At the beginning of the forecast period, $PM_{2.5}$ concentrations above 300 μg m^{-3} are found in Henan, Hebei, Hunan, and Hubei. During the forecast, most $PM_{2.5}$ is transported to the Pacific Ocean by a strong northwest wind. At the lead time of 32 h, $PM_{2.5}$ concentrations for most of the Chinese mainland fall below 150 μg m^{-3}, as shown in the top panel of Figure 2. For comparison, we estimated the forecast errors by the difference between the forecast and the assimilated concentrations, as shown in the middle panel of Figure 2. Accuracy of the assimilated data is verified in SI Section S4 and Figure S2. As is clear from Figure 2, forecast errors are transported along with concentrations, and large forecast errors occur mostly in heavily polluted areas. The transported initial errors, calculated by using the IETM approach, are shown in the bottom panel of Figure 2. The estimated forecast errors and the transported initial errors are identical by definition at the start of the forecast. During the forecast, the differences increase, but the transported errors consistently account for most of the estimated errors. The differences are likely attributable to uncertainties in the emissions, reactions, deposition, and wind fields. To sum up, these results confirm that forecast errors of $PM_{2.5}$ can be transported along with concentrations from the CTM and the transported errors have a strong impact on forecasts with a lead time up to 32 h.

To further demonstrate the importance of transport in the evolution of forecast errors, we decompose the forecast errors into two parts: the error transported from an hour ago and the other error that is generated during the last hour. Both parts of error involve uncertainties stemming from the CTM modules and the input data, thus forming a different decomposition from those usually discussed in the literature. As shown in SI Figure S1, the transported error outweighs the other error by a factor of 6.6. This result is consistent with the work of Skachko et al.,[32] which found that transport plays a major role in describing the evolution of model error for data assimilation.

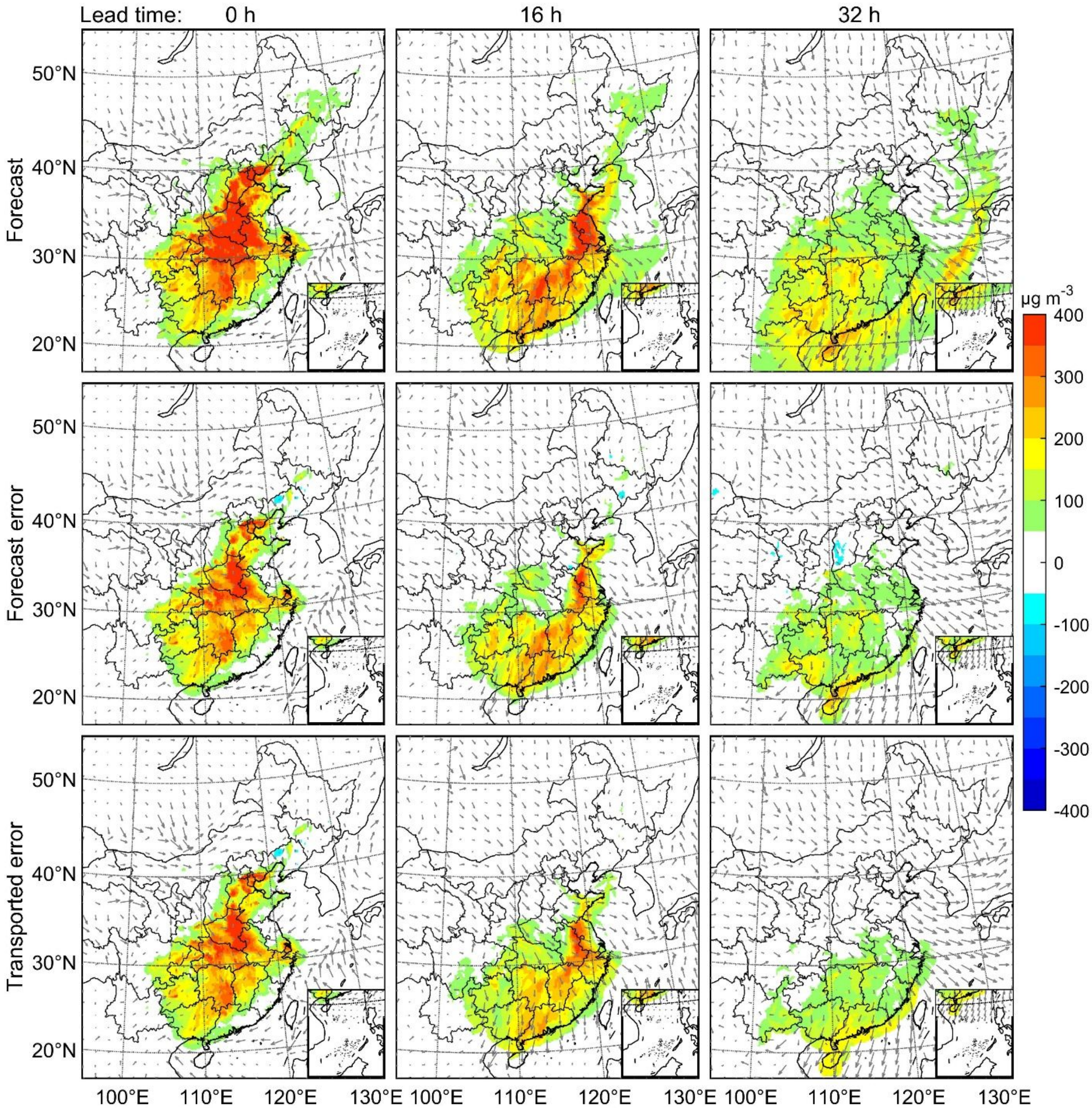

Figure 2. Illustrations of the transport of $PM_{2.5}$ forecast errors. The forecast starts at 20:00 on January 6, 2018. Forecast errors (middle) are estimated by the difference between the forecast (top) and assimilated concentrations. Transported errors (bottom) are calculated by using the IETM approach. An animated version of this figure is provided in SI Video S1.

Comparisons of Forecasting Methods

We compare the proposed IETM method with two commonly used forecasting schemes mentioned above, which we refer to as CTM forecasting with unassimilated ICs (CTMf) and that with assimilated ICs (CTMa). Three statistical measures are used to evaluate the accuracy of the forecasts: mean bias (MB), root-mean-square error (RMSE), and correlation coefficient ($\boldsymbol{r}$). Results for 1- to 4-day $PM_{2.5}$ forecasts during January 2018 using three methods over the study period are summarized in Table 1. Examples of the forecast $PM_{2.5}$ concentrations at three validation sites in the BTH, YRD, and PRD regions are shown in SI Figure S3.

As noted from Table 1, the CTMf method exhibits a large upward bias of 57.0–64.0 μg m^{-3} for 1- to 4-day forecasts over all validation sites. This overestimation could be largely explained by stringent emission controls that are not captured by the currently used emission inventory, such as strengthening industrial emissions standards, upgrading industrial boilers, phasing out outdated industrial capacities, and promoting clean fuels in the residential sector.

Table 1. Performance Statistics for 1- to 4-Day $PM_{2.5}$ Forecasts During January 2018 Using Three Methods[a]

region	method	1-day forecast			2-day forecast			3-day forecast			4-day forecast		
		MB	RMSE	***r***	MB	RMSE	***r***	MB	RMSE	***r***	MB	RMSE	***r***
all	CTMf	64.0	98.9	0.43	59.8	97.5	0.39	59.3	98.3	0.36	57.0	98.3	0.31
	CTMa	51.3	82.6	0.47	57.0	93.6	0.40	58.0	96.4	0.36	56.4	97.4	0.31
	IETM	15.8	47.7	0.58	31.1	70.5	0.39	41.9	81.9	0.34	47.2	88.9	0.29
BTH	CTMf	66.7	111.5	0.54	64.1	109.2	0.49	70.1	115.4	0.41	66.6	119.9	0.33
	CTMa	48.9	86.7	0.59	62.1	105.7	0.49	69.4	114.1	0.41	66.3	119.4	0.33
	IETM	22.6	60.5	0.61	51.2	94.3	0.46	64.9	108.4	0.41	64.4	117.1	0.33
YRD	CTMf	78.1	112.4	0.68	70.1	113.8	0.61	67.0	122.2	0.50	66.3	121.2	0.47
	CTMa	62.8	92.8	0.71	67.3	109.6	0.62	65.7	120.2	0.50	65.7	120.2	0.47
	IETM	21.5	53.1	0.73	38.6	81.2	0.60	51.9	103.6	0.48	58.6	110.0	0.46
PRD	CTMf	49.1	76.4	0.20	47.7	75.1	0.20	48.2	78.5	0.21	49.3	81.1	0.18
	CTMa	41.3	66.7	0.27	44.2	70.9	0.22	46.4	76.0	0.21	48.3	79.6	0.17
	IETM	1.6	34.8	0.60	-5.3	47.4	0.18	4.7	55.4	0.04	20.5	63.6	0.07

[a]BTH, Beijing-Tianjin-Hebei region; YRD, Yangtze River Delta region; PRD, Pearl River Delta region. MB, mean bias (μg m^{-3}); RMSE, root-mean-square error (μg m^{-3}); ***r***, correlation coefficient. The CTMf and CTMa methods refer to CTM forecasting with unassimilated and assimilated ICs, respectively, and IETM refers to CTMf corrected by the IETM output.

The CTMa method yields improved forecasting performance over CTMf by initializing the CTM with the assimilated data. As shown in Figure 3, the RMSE of 1-day forecasts using the CTMf method exceeds 150 μg m^{-3} at most validation sites in the Sichuan Basin, the North China Plain, and the Hubei–Hunan Plain, while RMSEs under 50 μg m^{-3} are found mainly in Northeast China, Northwest China, and Yunnan. A reduction of RMSE is clearly observed in areas with high RMSEs, especially the North China Plain. The RMSE of 1-day forecasts over all validation sites is lowered by 16.2 μg m^{-3}, amounting to a reduction of 16.4% (Table 1).

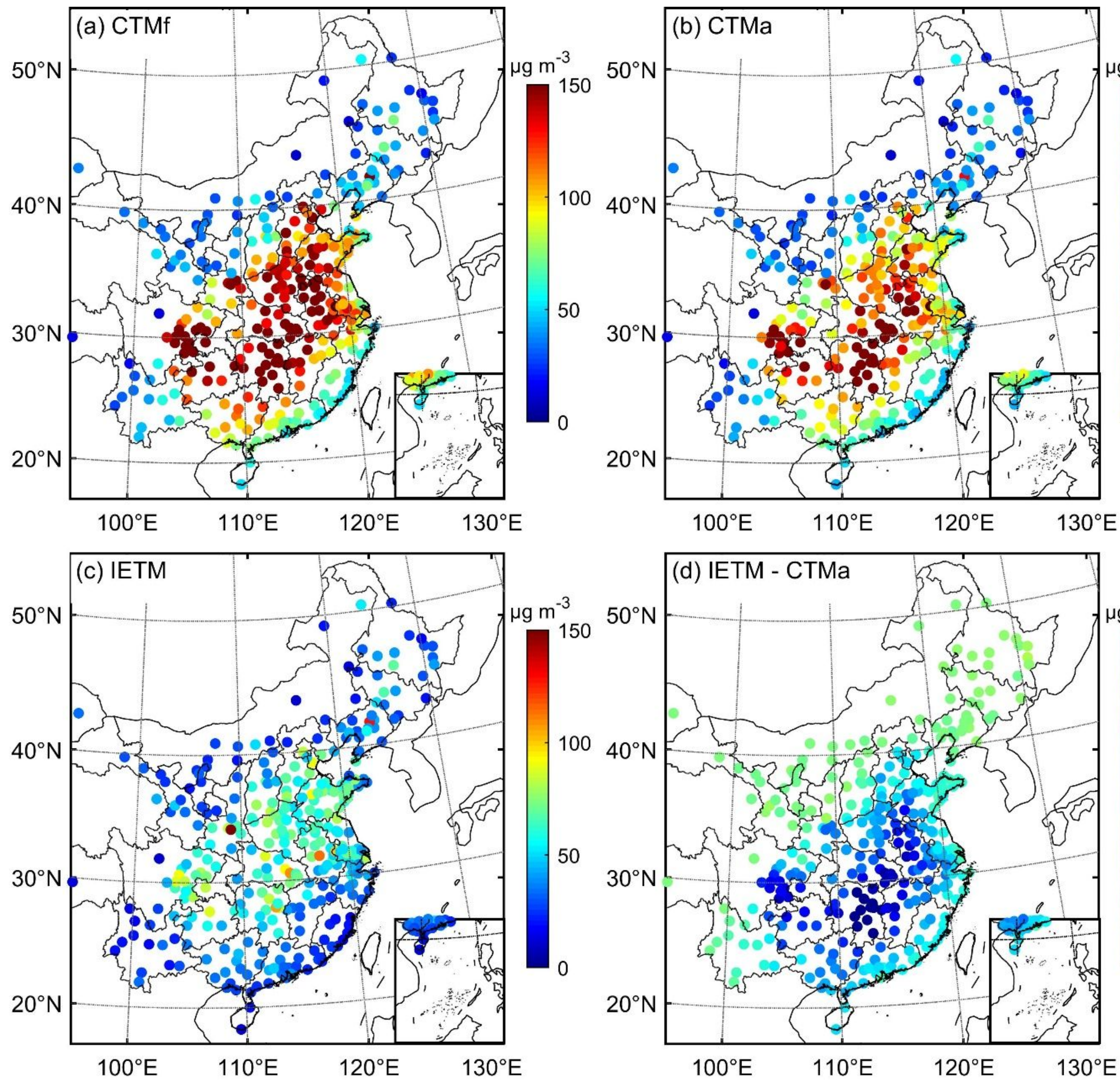

Figure 3. Maps of RMSE at validation sites for 1-day forecasts during January 2018. The RMSEs of the CTMf, CTMa, and IETM methods are shown in (a)–(c), respectively, and differences between the RMSEs of IETM and CTMa are shown in (d).

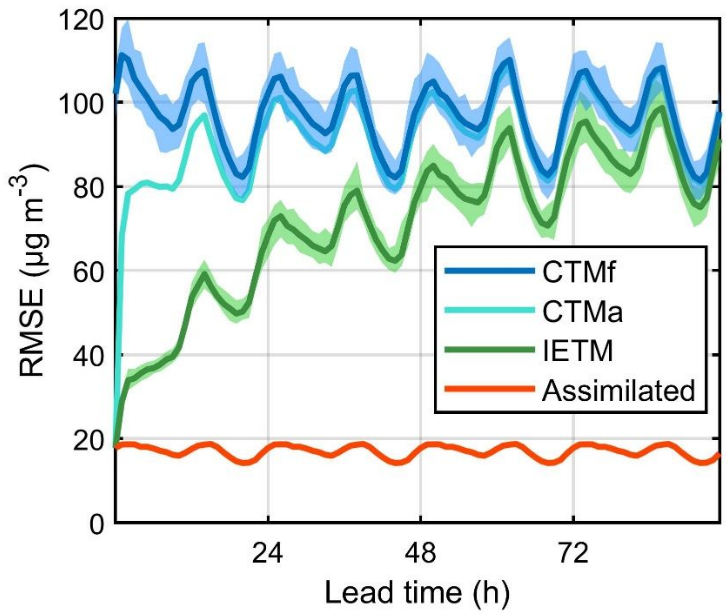

Figure 4. Curves of RMSE over all validation sites as functions of lead time for $PM_{2.5}$ forecasts during January 2018. Shaded areas around the curves for CTMa and IETM represent 95% confidence intervals, which are calculated by using the bootstrap method. The red line represents the RMSE of assimilated $PM_{2.5}$ from the CTM.

Although $PM_{2.5}$ forecasts are generally improved by the CTMa method, the benefits are largely limited to 1-day forecasts. At the beginning of the forecast, the RMSE for the CTMa method is substantially lower than that for CTMf, as evident from Figure 4. However, the RMSE for CTMa increases dramatically and its advantage over CTMf is quickly lost, especially during the first hour. A similar phenomenon in the first hour of the forecast was also noted by previous work,[19] where only observations of $PM_{2.5}$, but not its precursors, were assimilated. Compared with the relatively large improvement for 1-day forecasts, only reductions of 3.9, 1.9, and 0.9 μg m^{-3}, or 4.0%, 1.9%, and 0.9%, respectively, are obtained from the CTMa method for 2- to 4-day forecasts (Table 1). These results are consistent with previous studies suggesting that most improvements by assimilating surface $PM_{2.5}$ observations are limited to 1-day forecasts.[11-13]

By contrast, improvements from the IETM method tend to be more substantial and last longer. Starting with the same reduction in RMSE as that by CTMa, the IETM forecasts only see a gradual increase in RMSE during the first two days, and the impacts of assimilated ICs are still visible on the fourth day in Figure 4. A periodic diurnal variation in the RMSEs of all forecasts is noted in Figure 4, which is likely caused by uncertainties in the diurnal variation of emissions and meteorological conditions such as solar intensity, temperature, wind speed, and the height of the planetary boundary layer. As shown spatially in Figure 3, improvements in RMSE for 1-day forecasts by IETM over CTMa are apparent at most validation sites and more pronounced in areas with high RMSEs. Remarkably, while the RMSEs for validation sites in Guangdong, Fujian, and Zhejiang are scarcely reduced by CTMa, they are cut down to under 50 μg m^{-3} by the IETM method. Compared with the results for CTMf, the reductions in RMSE for 1- to 4-day forecasts by the IETM method are 51.2, 27.0, 16.4, and 9.4 μg m^{-3}, or 51.8%, 27.7%, 16.7%, and 9.5%, respectively, which are 3.2, 6.9, 8.6, and 10.4 times those by the CTMa method (Table 1). Table 1 also suggests that improvements by the IETM method are mainly in the MB and RMSE but less in the correlation coefficient, especially for 2- to 4-day forecasts. This inconsistency is due to the fact that r is a standardized measure that magnifies the contributions of locations with low concentrations and hence small forecast errors. The IETM approach, however, tends to transport large forecast errors to locations with small errors, which may decrease *r* for those locations and offset the improvement in *r* elsewhere. Nevertheless, since $PM_{2.5}$ concentrations and forecast errors show marked spatiotemporal variability, the MB and RMSE measures seem more appropriate for assessing predictive accuracy in this case.

To further test the robustness of our method for different periods and seasons, we applied it to the month of July 2017. Although the RMSE is much lower in the summer, the results show similar trends of improvement to those for January 2018. Notably, as shown in SI Figure S4, the RMSEs for 1-day forecasts in the Sichuan Basin are only slightly reduced by the CTMa method, but are cut by about a half with the IETM method. The reduced RMSEs for 1- to 4-day forecasts during July 2017 and January 2018 are compared in SI Figure S5, which demonstrate similar patterns and last up to 4 days. These results together suggest that the IETM method can yield amplified and prolonged improvement over commonly used forecasting schemes.

Model Balances in the Forecasts

It is useful to investigate the ways in which the proposed IETM method helps to mitigate the imbalance issue. Two types of imbalances can generally occur in the CTM due to data assimilation. The first type is the imbalance between the assimilated and unassimilated model variables.[16] Ideally, the calculation of chemical reactions should be more accurate with the assimilated ICs. In reality, however, only a few of the species involved in the CTM can be assimilated owing to the lack of observations. This inconsistency can thus disturb the balance of chemical reactions. As a result, improvements for the assimilated species may diminish quickly as the CTM tries to reach a new reaction balance. The second type is the imbalance in space.[17] For instance, in this study, the accuracy of ICs in the surface layer was improved by assimilating surface $PM_{2.5}$ observations, whereas $PM_{2.5}$ in the higher layers was not affected since no lidar or satellite data were assimilated. Such an imbalance may lead to spurious differences between the concentrations of $PM_{2.5}$ in the surface layer and in the adjacent layer. During the forecast, these spurious differences tend to be lessened by vertical transport in the CTM; however, the effects of data assimilation on surface $PM_{2.5}$ are also counteracted. Collectively, these two types of imbalances may cause spurious species interactions and vertical transport in the CTM, thereby diminishing the benefits from data assimilation.

The IETM method takes a fundamentally different way to extract information from the assimilated ICs. It calculates the transport of initial errors and corrects the baseline forecast accordingly. Neither of the two imbalance problems mentioned above will be encountered. First, the IETM does not explicitly involve any reaction process, thereby avoiding interactions between the assimilated and unassimilated species. Moreover, only the surface layer is considered in the IETM, so that no vertical imbalance will arise.

To verify the above arguments, we estimated the concentrations of $PM_{2.5}$ components using the IETM by assuming that the chemical composition of $PM_{2.5}$ is the same as that in the baseline CTM forecast. Results averaged over the YRD region for a 4-day period are shown in Figure 5. Since no precursors of $PM_{2.5}$ were assimilated in this study, chemical reactions between $PM_{2.5}$ components and their precursors were significantly disturbed in the CTMa method. As expected, the concentrations of highly reactive $PM_{2.5}$ components, including nitrate, ammonium, and sulfate, change abruptly in the first hour and become indistinguishable from the CTMf forecasts (Figure 5b–d). By contrast, improvements for these components by the IETM method are consistently large and can last up to four days. Similar trends are found for those less reactive components, including organic aerosols, black carbon, and other $PM_{2.5}$ components (Figure 5e–g). In this case, it is interesting to note that, although the CTMa forecasts converge to those by CTMf and the effects of data assimilation almost disappear within a day, the changes are not as abrupt as those for highly reactive components. This difference suggests that vertical transport may play a major role for these components, which takes a longer time to reach a dynamic balance. The relatively longer duration of assimilation effect may also be attributed to the start time of 20:00 and weaker vertical transport in the nighttime. In summary, improvements by the IETM method are substantial and consistent across all components of $PM_{2.5}$, and are not affected by either spurious species interactions or vertical transport.

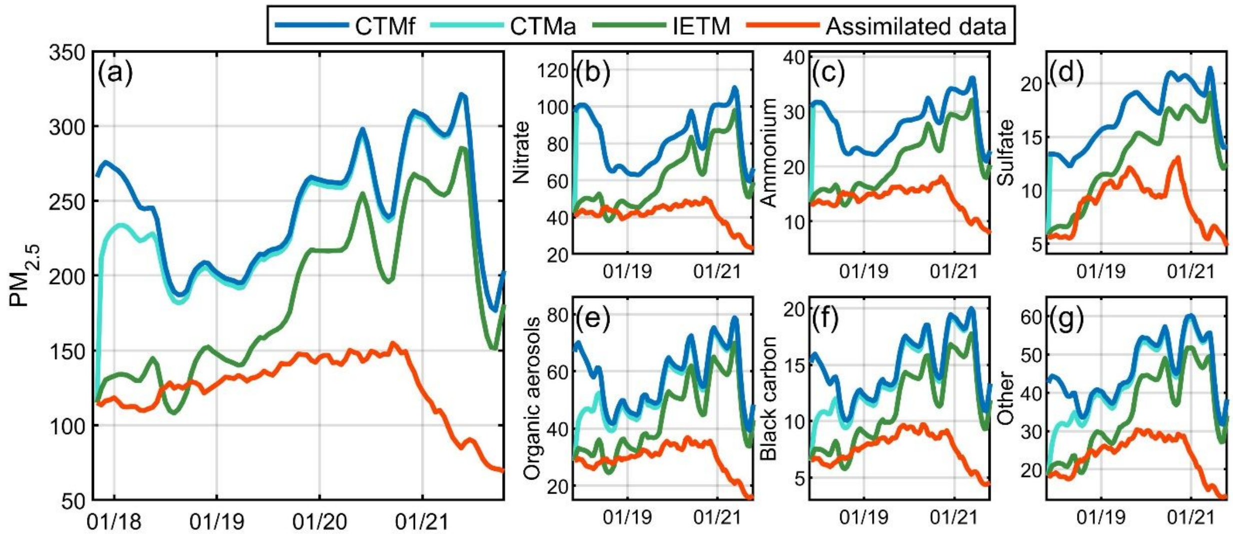

Figure 5. Time series of the CTMf, CTMa, and IETM forecasts of total $PM_{2.5}$ (a) and its components (b–g) over the Yangtze River Delta region. The forecast starts at 20:00 on January 17, 2018.

Limitations and Possible Extensions

Fully exploiting the benefits of data assimilation is crucial for improving air quality forecasting. Our proposed method provides a reliable, flexible way to enhance and extend the impacts of the assimilated data without being affected by the imbalance issue. The methodology is easy to implement and highly efficient as it does not require expensive CTM computations or complex initialization strategies. Nevertheless, the IETM assumes that the lifetime of $PM_{2.5}$ forecast errors is prespecified and vertical transport is negligible. Although these assumptions affect only the calculated impacts of assimilated ICs and seem plausible in most cases, there are exceptions. For instance, scavenging of $PM_{2.5}$ by precipitation would result in a shorter lifetime of $PM_{2.5}$. Besides, when air masses collide or wildfires occur, vertical transport may play a more important role and should not be ignored. Moreover, since the IETM trades model complexity for model balance, its advantages over direct initialization techniques would diminish as the number of species and vertical coverage in the assimilated data increase.

The IETM method could be extended in many ways to deal with these limitations. For example, a more sophisticated decay scheme, incorporating the reaction and deposition processes, could be developed, which would provide better predictions over areas and periods with unusual $PM_{2.5}$ lifetimes. Moreover, the forecast errors that are not explained by the transport or decay of initial errors could be modeled using statistical or machine learning methods, which is likely to yield further improvement for longer-range forecasts.

ASSOCIATED CONTENT

Supporting Information

Detailed descriptions of the CTM and data assimilation method, implementation of horizontal advection, validation of assimilation results, supplementary figures (PDF)

Animation of the transport of $PM_{2.5}$ forecast errors (Video S1) (AVI)

AUTHOR INFORMATION

Corresponding Authors

*Email: wuhuangjian@pku.edu.cn

*Email: weilin@math.pku.edu.cn

Notes

The authors declare no competing financial interest.

ACKNOWLEDGMENTS

This work was supported by National Key R&D Program of China grants 2016YFC0207703, 2016YFC0207701, 2018YFC0213106, and 2018YFC0213100, National Natural Science Foundation of China grants 11671018, 71532001, 91644216, and 41705108, Beijing Natural Science Foundation grant Z190001, and Beijing Academy of Artificial Intelligence.

REFERENCES

(1) Zhang, Y.; Bocquet, M.; Mallet, V.; Seigneur, C.; Baklanov, A. Real-time air quality forecasting, part I: History, techniques, and current status. *Atmos. Environ.* **2012**, *60*, 632-655.

(2) Kumar, R.; Peuch, V.-H.; Crawford, J. H.; Brasseur, G. Five steps to improve air-quality forecasts. *Nature* **2018**, *561* (7721), 27-29.

(3) Zhang, Q.; Zheng, Y.; Tong, D.; Shao, M.; Wang, S.; Zhang, Y.; Xu, X.; Wang, J.; He, H.; Liu, W.; Ding, Y.; Lei, Y.; Li, J. H.; Wang, Z.; Zhang, X.; Wang, Y.; Cheng, J.; Liu, Y.; Shi, Q.; Yan, L.; Geng, G.; Hong, C.; Li, M.; Liu, F.; Zheng, B.; Cao, J.; Ding, A.; Gao, J.; Fu, Q.; Huo, J.; Liu, B.; Liu, Z.; Yang, F.; He, K.; Hao, J. Drivers of improved $PM_{2.5}$ air quality in China from 2013 to 2017. *Proc. Natl. Acad. Sci. U.S.A.* **2019**, *116* (49), 24463-24469.

(4) Daley, R., *Atmospheric Data Analysis*. Cambridge University Press: Cambridge, U.K., 1991.

(5) Talagrand, O.; Courtier, P. Variational assimilation of meteorological observations with the adjoint vorticity equation. I: Theory. *Q. J. R. Meteorol. Soc.* **1987**, *113* (478), 1311-1328.

(6) Evensen, G. Sequential data assimilation with a nonlinear quasi-geostrophic model using Monte Carlo methods to forecast error statistics. *J. Geophys. Res.* **1994**, *99* (C5), 10143-10162.

(7) Bocquet, M.; Elbern, H.; Eskes, H.; Hirtl, M.; Žabkar, R.; Carmichael, G. R.; Flemming, J.; Inness, A.; Pagowski, M.; Camaño, J. L. P.; Saide, P. E.; San Jose, R.; Sofiev, M.; Vira, J.; Baklanov, A.; Carnevale, C.; Grell, G.; Seigneur, C. Data assimilation in atmospheric chemistry models: current status and future prospects for coupled chemistry meteorology models. *Atmos. Chem. Phys.* **2015**, *15* (10), 5325-5358.

(8) Peng, Z.; Lei, L.; Liu, Z.; Su, J.; Ding, A.; Ban, J.; Chen, D.; Kou, X.; Chu, K. The impact of multi-species surface chemical observation assimilation on air quality forecasts in China. *Atmos. Chem. Phys.* **2018**, *18* (23), 17387-17404.

(9) Cheng, X.; Liu, Y.; Xu, X.; You, W.; Zang, Z.; Gao, L.; Chen, Y.; Su, D.; Yan, P. Lidar data assimilation method based on CRTM and WRF-Chem models and its application in $PM_{2.5}$ forecasts in Beijing. *Sci. Total Environ.* **2019**, *682*, 541-552.

(10) Saide, P. E.; Kim, J.; Song, C. H.; Choi, M.; Cheng, Y.; Carmichael, G. R. Assimilation of next generation geostationary aerosol optical depth retrievals to improve air quality simulations. *Geophys. Res. Lett.* **2014**, *41* (24), 9188-9196.

(11) Ma, C.; Wang, T.; Zang, Z.; Li, Z. Comparisons of three-dimensional variational data assimilation and model output statistics in improving atmospheric chemistry forecasts. *Adv. Atmos. Sci.* **2018**, *35* (7), 813-825.

(12) Li, Z.; Zang, Z.; Li, Q. B.; Chao, Y.; Chen, D.; Ye, Z.; Liu, Y.; Liou, K. N. A three-dimensional variational data assimilation system for multiple aerosol species with WRF/Chem and an application to $PM_{2.5}$ prediction. *Atmos. Chem. Phys.* **2013**, *13* (8), 4265-4278.

(13) Feng, S.; Jiang, F.; Jiang, Z.; Wang, H.; Cai, Z.; Zhang, L. Impact of 3DVAR assimilation of surface $PM_{2.5}$ observations on $PM_{2.5}$ forecasts over China during wintertime. *Atmos. Environ.* **2018**, *187*, 34-49.

(14) Textor, C.; Schulz, M.; Guibert, S.; Kinne, S.; Balkanski, Y.; Bauer, S.; Berntsen, T.; Berglen, T.; Boucher, O.; Chin, M.; Dentener, F.; Diehl, T.; Easter, R.; Feichter, H.; Fillmore, D.; Ghan, S.; Ginoux, P.; Gong, S.; Grini, A.; Hendricks, J.; Horowitz, L.; Huang, P.; Isaksen, I.; Iversen, I.; Kloster, S.; Koch, D.; Kirkevåg, A.; Kristjansson, J. E.; Krol, M.; Lauer, A.; Lamarque, J. F.; Liu, X.; Montanaro, V.; Myhre, G.; Penner, J.; Pitari, G.; Reddy, S.; Seland, Ø.; Stier, P.; Takemura, T.; Tie, X. Analysis and quantification of the diversities of aerosol life cycles within AeroCom. *Atmos. Chem. Phys.* **2006**, *6* (7), 1777-1813.

(15) Croft, B.; Pierce, J. R.; Martin, R. V. Interpreting aerosol lifetimes using the GEOS-Chem model and constraints from radionuclide measurements. *Atmos. Chem. Phys.* **2014**, *14* (8), 4313-4325.

(16) Weaver, A. T.; Deltel, C.; Machu, E.; Ricci, S.; Daget, N. A multivariate balance operator for variational ocean data assimilation. *Q. J. R. Meteorol. Soc.* **2005**, *131* (613), 3605-3625.

(17) Greybush, S. J.; Kalnay, E.; Miyoshi, T.; Ide, K.; Hunt, B. R. Balance and Ensemble Kalman Filter Localization Techniques. *Mon. Weather Rev.* **2011**, *139* (2), 511-522.

(18) Carrassi, A.; Bocquet, M.; Bertino, L.; Evensen, G. Data assimilation in the geosciences: An overview of methods, issues, and perspectives. *WIREs Clim. Change* **2018**, *9* (5), No. e535.

(19) Schwartz, C. S.; Liu, Z.; Lin, H.-C.; McKeen, S. A. Simultaneous three-dimensional variational assimilation of surface fine particulate matter and MODIS aerosol optical depth. *J. Geophys. Res.* **2012**, *117* (D13), No. D13202.

(20) Zheng, H.; Liu, J.; Tang, X.; Wang, Z.; Wu, H.; Yan, P.; Wang, W. Improvement of the Real-time $PM_{2.5}$ Forecast over the Beijing-Tianjin-Hebei Region using an Optimal Interpolation Data Assimilation Method. *Aerosol Air Qual. Res.* **2018**, *18* (5), 1305-1316.

(21) Balmaseda, M.; Anderson, D. Impact of initialization strategies and observations on seasonal forecast skill. *Geophys. Res. Lett.* **2009**, *36* (1), No. L01701.

(22) Mulholland, D. P.; Laloyaux, P.; Haines, K.; Balmaseda, M. A. Origin and Impact of Initialization Shocks in Coupled Atmosphere–Ocean Forecasts. *Mon. Weather Rev.* **2015**, *143* (11), 4631-4644.

(23) Machenhauer, B. On the Dynamics of Gravity Oscillations in a Shallow Water Model, with Applications to Normal Mode Initialization. *Contrib. Atmos. Phys.* **1977**, *50*, 253-271.

(24) Baer, F.; Tribbia, J. J. On Complete Filtering of Gravity Modes Through Nonlinear Initialization. *Mon. Weather Rev.* **1977**, *105* (12), 1536-1539.

(25) Lynch, P.; Huang, X.-Y. Initialization of the HIRLAM Model Using a Digital Filter. *Mon. Weather Rev.* **1992**, *120* (6), 1019-1034.

(26) Bloom, S. C.; Takacs, L. L.; da Silva, A. M.; Ledvina, D. Data Assimilation Using Incremental Analysis Updates. *Mon. Weather Rev.* **1996**, *124* (6), 1256-1271.

(27) Williamson, D. L.; Daley, R.; Schlatter, T. W. The Balance between Mass and Wind Fields Resulting from Multivariate Optimal Interpolation. *Mon. Weather Rev.* **1981**, *109* (11), 2357-2376.

(28) Errico, R. M.; Rosmond, T. E.; Goerss, J. S. A Comparison of Analysis and Initialization Increments in an Operational Data-Assimilation System. *Mon. Weather Rev.* **1993**, *121* (2), 579-588.

(29) Keller, C. A.; Evans, M. J. Application of random forest regression to the calculation of gas-phase chemistry within the GEOS-Chem chemistry model v10. *Geosci. Model Dev.* **2019**, *12* (3), 1209-1225.
(30) Bauer, P.; Thorpe, A.; Brunet, G. The quiet revolution of numerical weather prediction. *Nature* **2015**, *525* (7567), 47-55.
(31) Kristiansen, N. I.; Stohl, A.; Olivié, D. J. L.; Croft, B.; Søvde, O. A.; Klein, H.; Christoudias, T.; Kunkel, D.; Leadbetter, S. J.; Lee, Y. H.; Zhang, K.; Tsigaridis, K.; Bergman, T.; Evangeliou, N.; Wang, H.; Ma, P.-L.; Easter, R. C.; Rasch, P. J.; Liu, X.; Pitari, G.; Di Genova, G.; Zhao, S. Y.; Balkanski, Y.; Bauer, S. E.; Faluvegi, G. S.; Kokkola, H.; Martin, R. V.; Pierce, J. R.; Schulz, M.; Shindell, D.; Tost, H.; Zhang, H. Evaluation of observed and modelled aerosol lifetimes using radioactive tracers of opportunity and an ensemble of 19 global models. *Atmos. Chem. Phys.* **2016**, *16* (5), 3525-3561.
(32) Skachko, S.; Ménard, R.; Errera, Q.; Christophe, Y.; Chabrillat, S. EnKF and 4D-Var data assimilation with chemical transport model BASCOE (version 05.06). *Geosci. Model Dev.* **2016**, *9* (8), 2893-2908.
(33) Liu, X.; Yeo, K.; Hwang, Y.; Singh, J.; Kalagnanam, J. A statistical modeling approach for air quality data based on physical dispersion processes and tts application to ozone modeling. *Ann. Appl. Stat.* **2016**, *10* (2), 756-785.
(34) Wang, Z.; Maeda, T.; Hayashi, M.; Hsiao, L.-F.; Liu, K.-Y. A Nested Air Quality Prediction Modeling System for Urban and Regional Scales: Application for High-Ozone Episode in Taiwan. *Water Air Soil Pollut.* **2001**, *130* (1-4), 391-396.
(35) Walcek, C. J.; Aleksic, N. M. A simple but accurate mass conservative, peak-preserving, mixing ratio bounded advection algorithm with Fortran code. *Atmos. Environ.* **1998**, *32* (22), 3863-3880.
(36) Jacobson, M. Z. GATOR-GCMM: A global- through urban-scale air pollution and weather forecast model 1. Model design and treatment of subgrid soil, vegetation, roads, rooftops, water, sea ice, and snow. *J. Geophys. Res.* **2001**, *106* (D6), 5385-5401.
(37) Kadowaki, M.; Katata, G.; Terada, H.; Nagai, H. Development of the Eulerian atmospheric transport model GEARN-FDM: Validation against the European tracer experiment. *Atmos. Pollut. Res.* **2017**, *8* (2), 394-402.
(38) Smagorinsky, J. General circulation experiments with the primitive equations: I. The basic experiment. *Mon. Weather Rev.* **1963**, *91* (3), 99-164.
(39) Wu, H.; Tang, X.; Wang, Z.; Wu, L.; Lu, M.; Wei, L.; Zhu, J. Probabilistic Automatic Outlier Detection for Surface Air Quality Measurements from the China National Environmental Monitoring Network. *Adv. Atmos. Sci.* **2018**, *35* (12), 1522-1532.
(40) Liu, J.; Mauzerall, D. L.; Horowitz, L. W.; Ginoux, P.; Fiore, A. M. Evaluating inter-continental transport of fine aerosols: (1) Methodology, global aerosol distribution and optical depth. *Atmos. Environ.* **2009**, *43* (28), 4327-4338.
(41) Anenberg, S. C.; West, J. J.; Yu, H.; Chin, M.; Schulz, M.; Bergmann, D.; Bey, I.; Bian, H.; Diehl, T.; Fiore, A.; Hess, P.; Marmer, E.; Montanaro, V.; Park, R.; Shindell, D.; Takemura,

T.; Dentener, F. Impacts of intercontinental transport of anthropogenic fine particulate matter on human mortality. *Air Qual. Atmos. Health* **2014**, *7* (3), 369-379.

(42) Chin, M.; Diehl, T.; Ginoux, P.; Malm, W. Intercontinental transport of pollution and dust aerosols: implications for regional air quality. *Atmos. Chem. Phys.* **2007**, *7* (21), 5501-5517.

(43) Wang, J.; Zhang, M.; Bai, X.; Tan, H.; Li, S.; Liu, J.; Zhang, R.; Wolters, M. A.; Qin, X.; Zhang, M.; Lin, H.; Li, Y.; Li, J.; Chen, L. Large-scale transport of $PM_{2.5}$ in the lower troposphere during winter cold surges in China. *Sci. Rep.* **2017**, *7*, No. 13238.

(44) Yu, H.; Remer, L. A.; Chin, M.; Bian, H.; Tan, Q.; Yuan, T.; Zhang, Y. Aerosols from overseas rival domestic emissions over North America. *Science* **2012**, *337* (6094), 566-569.

TOC Art

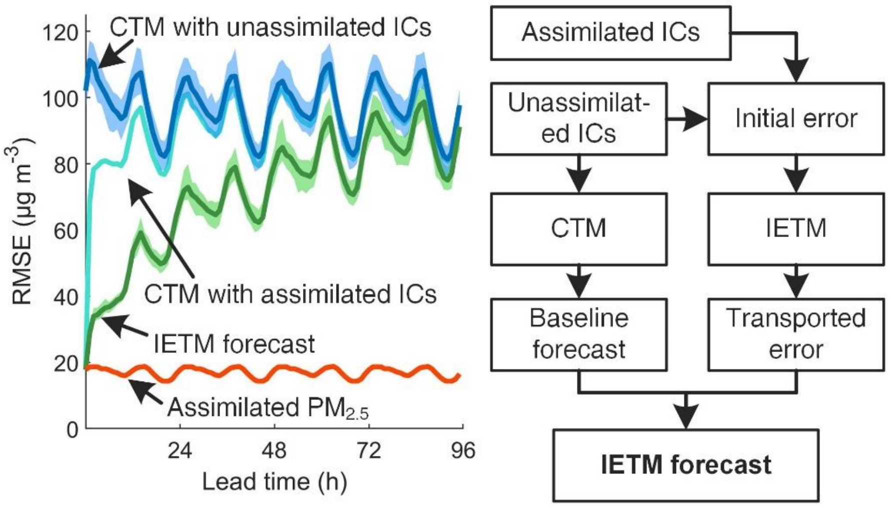

(For Table of Contents Only)